 CMES, vol.93, no.1, pp.69-90, 2013

Half Space Acoustic Problems Analysis by Fast Multipole Boundary Face Method

Xianhui Wang[1], Jianming Zhang[1,2], Xingshuai Zheng[1], Fenglin Zhou[1]

Abstract: In this paper, a half space adaptive fast multipole boundary face method (FMBFM) is presented for solving the three-dimensional half space exterior acoustic problems. In the presented method, the Burton-Miller equation based on the conventional boundary integral equation (CBIE) and its hyper-singular boundary integral equation (HBIE) is used to deal with the fictitious eigenfrequencies problem. The half space Green's function is employed, thus the tree structure in the fast multipole method can be used only for the real domain. The higher order elements and an adaptive tree structure are used to improve the efficiency of the FMBFM. This half space adaptive FMBFM for half space acoustic problems is an extension of the adaptive FMBFM for full space acoustic problems developed by the authors. Numerical examples for half space acoustic problems in this paper demonstrate the efficiency and validity of this method.

Keywords: fast multipole boundary face method, Burton-Miller equation, acoustic problems, half space, modified hyper-singular boundary integral equation

1 Introduction

Acoustic problems in half space are a major subject in engineering. Many research works have been done on this aspect (Seybert et al., 1988; Seçgin et al., 2010; Cao et al., 2010). The half space Green's function (Seybert et al., 1988) can be applied by adding the source solution at the image point to the original full-space Green's function for dealing with half space problems. Sound source localization and identification of a refrigerator were accomplished by using the half space boundary element method (BEM) (Seçgin et al., 2010). Using the half space Green's function, the discretization of the rigid infinite plane is removed and only the boundaries

[1] State Key Laboratory of Advanced Design and Manufacturing for Vehicle Body, College of Mechanical and Vehicle Engineering, Hunan University, Changsha 410082, China.
[2] Corresponding Author.
Tel: 86 731 88823061; Fax: +86-731-88822051; Email: zhangjianm@gmail.com

of the structure need to be discretized. However, the computational scale in these study all are relatively small.

The boundary face method (BFM) (Zhang et al., 2009; Qin et al., 2010), based on the boundary integral equation, is a numerical method. It is a generalization of the conventional BEM and boundary node method (Mukherjee et al., 1997; Zhang et al., 2001). The BFM is implemented directly using the boundary representation (B-rep) data structure that is used in most CAD packages for geometry modeling. The Sommerfeld radiation condition for acoustic exterior problems in BFM at infinity can be satisfied automatically. All these advantages make the BFM an attractive candidate for analyzing the exterior acoustic problems. Several works have been published to improve or extend the applicability of the BFM (Gu et al., 2011; Zhou et al., 2011).

The fast multipole method (FMM) (Rokhlin, 1985; Greengard, 1987) is employed to improve the effective of the BFM in this paper. Some of the research on fast multipole fast multipole boundary integral equation method can be found in Refs. (Aoki, et al., 2004; Brancati et al., 2009; Chen, et al. 2001; Wang, et al. 2005; Wang, et al. 2012; Qian, et al. 2013).The applications of FMM for acoustic problems have been more than 20 years. Rokhlin proposed a diagonal formed FMM for Helmholtz equation (Rokhlin, 1993). A huge improvement could be provided in the efficiency of the FMM. Shen proposed an adaptive FMM for 3-D full space acoustic problems (Shen et al., 2007). The performance of adaptive FMM algorithm can be several times faster than that of the non-adaptive one. An adaptive algorithm for the fast multipole BEM based on a new definition of the interaction list is proposed (Bapat et al., 2010). This algorithm can reduce the moment-to-local (M2L) translations by about 30-40% and therefore improve the efficiency for the FMM. An analytical integration method is given by Wu to compute the moments in the diagonal form FMM (Wu et al., 2012). A comparison of the fast multipole with hierarchical matrices for the Helmholtz integral equation is presented (Brunner, et al. 2010). An investigation of the FMM for the Helmholtz equation with complex frequency is given (Frangi, et al. 2010). An adaptive fast multipole boundary face method (Wang et al., 2013) with higher order elements for 3D full space acoustic problems is presented by Wang. Bapat applied the adaptive FMM for 3D half space acoustic problems (Bapat et al., 2009). Using the half-space Green's function, only the local expansion is different from that for 3D full space FMM. The total CPU time and memory storage are also reduced by about a half for large scale half space acoustic problems. However, in this half space adaptive FMM, only the CBIE is used, thus the presented method can not get unique solution for the exterior acoustic problems at the fictitious frequencies.

In this paper, a half space adaptive fast multipole boundary face method (FMBFM)

based on the Burton-Miller equation (Burton et al., 1971) is presented for half space acoustic problems in 3D. The half space Green's function is employed in this study. The Burton-Miller equation, which is widely used in exterior full space acoustic problems, is rarely used in exterior half space acoustic problems. However, in this paper, a Burton-Miller equation based on the CBIE and its HBIE is used to deal with the problem of non unique solution. In the half space adaptive FMBFM, the analytical integrations cannot be performed, thus we employed higher order elements to improve the accuracy and efficiency. The FMBFM has been integrated into the widely used commercial CAD package UG-NX, and thus it is able to handle problems with complicated geometries. The tree data structure (Zhang et al., 2006), which is used in full space adaptive FMBFM, will be used in this half space adaptive FMBFM.

The paper is organized as follows: Section 2 mainly reviews the BIEs and the BFM for the acoustic wave problems. In Section 3, the multipole expansion formulations are described followed by several numerical examples which are given to demonstrate the efficiency and validity of the present FMBFM in Section 4. The paper ends with conclusions in Section 5.

2 The BIE formulations and the BFM

2.1 The BIE formulations for acoustic problems

The integral representation of the solution to the Helmholtz equation is:

$$c(P_0)\varphi(P_0) = \int_S G(P_0,P_0^{'},P)q(P)dS(P) - \int_S \frac{\partial G(P_0,P_0^{'},P)}{\partial n}\varphi(P)dS(P) + \varphi^I(P_0), \tag{1}$$

here

$$G(P_0,P_0^{'},P) = \frac{e^{ikr}}{4\pi r} + \frac{e^{ikr'}}{4\pi r'} \tag{2}$$

in which r is the distance between source point P_0 and field point P. r' is the distance between point $P_0^{'}$ and field point P. $P_0^{'}$ is mirror image point of source point P_0 (Fig. 1). For a soft infinite symmetry plane, the plus sign in $G(P_0,P_0^{'},P)$ should be changed to a minus sign. $\varphi^I(P_0)$ denotes a prescribed incident wave but it does not exist in radiation problems. $c(P_0)$=1/2 if the surface S is smooth around source point P_0. E is the exterior region (acoustic medium). $V$is the interior region (a body or scatter). The Eq. (1) is called as CBIE.

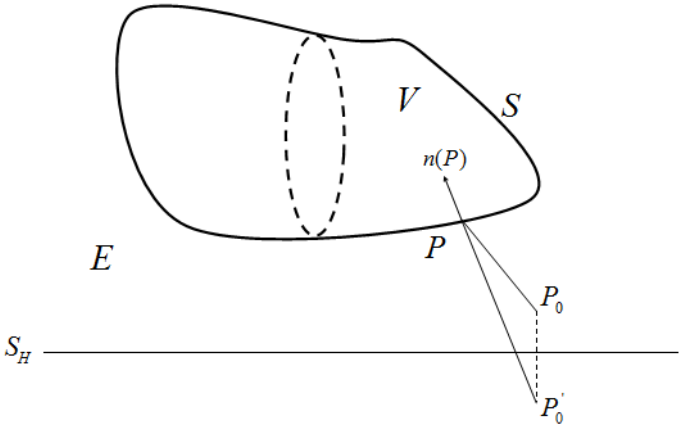

Figure 1: The graphic of half space problems

The boundary conditions for the governing equation of acoustic wave problems can be described as:

$$\begin{cases} Dirichlet \quad type \quad \phi = \bar{\phi}, \quad \forall x \in S \\ Neumann \quad type \quad q = \frac{\partial \phi}{\partial n} = \bar{q} = ikc\rho v_n, \quad \forall x \in S \\ Impedance \quad type \quad \phi = Zv_n, \quad \forall x \in S \end{cases}, \tag{3}$$

where c denotes the sound velocity in medium. .ρ is the mass density. v_n is the normal velocity. n is the outward normal. Z denotes the specific acoustic impedance. The quantities with overline indicate given values. $i = \sqrt{-1}$.

It is worth noting that $q(P)$=0 and $\phi(P)$=0 if the body V is contact with the plane S_H since they are not in the acoustic medium.

Based on the CBIE, its HBIE can be given as the following forms:

$$c(P_0)\frac{\partial \phi(P_0)}{\partial n_0} = \int_S \frac{\partial G(P_0, P_0', P)}{\partial n_0} \frac{\partial \phi(P)}{\partial n} dS(P) - \int_S \frac{\partial^2 G(P_0, P_0', P)}{\partial n \partial n_0} \phi(P) dS(P) + \frac{\partial \phi^I(P_0)}{\partial n_0},$$

$$P_0 \in S, \tag{4}$$

here n_0 is the outward normal at source point P_0. We set

$$\begin{cases} G(P_0, P) = \frac{e^{ikr}}{4\pi r} \\ G(P_0, P) = \frac{e^{ikr'}}{4\pi r'} \end{cases}, \tag{5}$$

and we reset the represent $\frac{\partial G(P_0,P_0^{'},P)}{\partial n_0}$ as the following forms:

$$\frac{\partial G(P_0,P_0^{'},P)}{\partial n_0}=\frac{\partial G(P_0,P)}{\partial n_0}+\frac{\partial G(P_0^{'},P)}{\partial n_0^{'}}, \tag{6}$$

here $n_0^{'}$ is the mirror image normal of n_0. For example, if the half space plane is z=0, and $n_0=(0,0,1)$, then $n_0^{'}=(0,0,-1)$.

As the weakly singular form of the HBIE (Liu et al., 1999), the hyper-singular integral integrand for half space problems can be given in the following weakly singular forms:

$$\begin{aligned}
&\int_S \frac{\partial^2 G(P_0,P_0^{'},P)}{\partial n\partial n_0}\phi(P)dS(P)\\
&=\int_S [\frac{\partial^2 G(P_0,P)}{\partial n\partial n_0}-\frac{\partial^2 G_0(P_0,P)}{\partial n\partial n_0}]\phi(P)dS(P)+\int_S \frac{\partial^2 G(P_0^{'},P)}{\partial n\partial n_0^{'}}\phi(P)dS(P)\\
&+\int_S \frac{\partial^2 G_0(P_0,P)}{\partial n\partial n_0}[\phi(P)-\phi(P_0)-\frac{\partial \phi}{\partial t_\alpha}(P_0)(t_\alpha-t_{0\alpha})]\phi(P)dS(P)\\
&+e_{\alpha k}\frac{\partial \phi}{\partial t_\alpha}(P_0)\int_S [\frac{\partial G_0(P_0,P)}{\partial n_0}n_k(P)+\frac{\partial G_0(P_0,P)}{\partial n}n_k(P_0)]dS(P),
\end{aligned} \tag{7}$$

here $G_0(P_0,P)=1/4\pi r$, t_α and $t_{0\alpha}$ are parametric coordinates of P and P_0, respectively, α=1,2. k=1, 2, 3.

Based on the Burton-Miller equation (Burton et al.), a complex linear combination (CHBIE) of the CBIE (1) and HBIE (4) is obtained to yield a unique solution for all the wave numbers:

$$\begin{aligned}
&\beta\left[\int_S \frac{\partial^2 G(P_0,P_0^{'},P)}{\partial n\partial n_0}\phi(P)dS(P)\right]+\int_S \frac{\partial G(P_0,P_0^{'},P)}{\partial n}\phi(P)dS(P)+c(P_0)\phi(P_0)\\
&=\beta\left[\int_S \frac{\partial G(P_0,P_0^{'},P)}{\partial n_0}\frac{\partial \phi(P)}{\partial n}dS(P)-c(P_0)\frac{\partial \phi(P_0)}{\partial n_0}\right]\\
&+\int_S G(P_0,P_0^{'},P)\frac{\partial \phi(P)}{\partial n}dS(P)+\beta\frac{\partial \phi^I(P_0)}{\partial n_0}+\phi^I(P_0)
\end{aligned}$$

$$\forall P_0\in S, \tag{8}$$

β=i/k is used as the imaginary coupling parameter of the Burton-Miller's formulation (Meyer et al., 1978), k is the wave number. Since the hypersingular integral has been converted to a weakly singular form, thus we could calculate all the integrals directly in the Burton-Miller equation.

2.2 The BFM for acoustic problems

As in the BEM, only the boundary discretization is required in the BFM for acoustic problems. The essential difference between BFM and BEM is that boundary elements are defined in different spaces. Namely, elements employed in BFM locate in the two-dimensional parametric space of the boundary surface. While in the BEM, elements locate in the three-dimensional physical space. In addition, the elements in BFM are only for integral computation. However, in BEM, the elements must be used for integral computation, variable interpolation and computing model approximation.

By dividing the boundary S into M elements and applying the shape functions on the element, we have the following approximations for variation of pressure and velocity:

$$\begin{cases} \phi(P) = \sum\limits_{k=1}^{N^E} N_k(P)\phi_k = \sum\limits_{k=1}^{N^E} N_k(t_1,t_2)\phi_k, \\ q(P) = \sum\limits_{k=1}^{N^E} N_k(P)q_k = \sum\limits_{k=1}^{N^E} N_k(t_1,t_2)q_k, \end{cases} \tag{9}$$

where ϕ_k and q_k denote the value of ϕ and q at the kth node, respectively. $N_k(.)$ is the serendipity quadratic shape function associated with the kth node, which is defined in the two-dimensional parametric space. N^E is the number of nodes in the element.

The discretized form of the Eq. (8) can be obtained as the following forms:

$$\sum_{j=1}^{M}\sum_{\alpha=1}^{N^E} h_{ij}^{\alpha}\phi_{\alpha} = \sum_{j=1}^{M}\sum_{\alpha=1}^{N^E} g_{ij}^{\alpha}q_{\alpha} + b_i, \text{ for node } i = 1,2,\ldots N, \tag{10}$$

here b_i is from the incident wave for the scattering problems, N denotes the total number of nodes, and

$$\begin{cases} h_{ij}^{\alpha}\phi_{\alpha} = \left[\beta \int_{S_j} \frac{\partial^2 G(P_i,P_i',P)}{\partial n(P)\partial n(P_i)} N_{\alpha}(P)dS(P) + \int_{S_j} \frac{\partial G(P_i,P_i',P)}{\partial n(P)} N_{\alpha}(P)dS(P) + \sigma(P_i,P_{\alpha})c(P_i)\right]\phi_{\alpha} \\ g_{ij}^{\alpha}q_{\alpha} = \left[\beta \int_{S_j} \frac{\partial G(P_i,P_i',P)}{\partial n(P_i)} N_{\alpha}(P)dS(P) + \int_{S_j} G(P_i,P_i',P)N_{\alpha}(P)dS(P) - \sigma(P_i,P_{\alpha})\beta c(P_i)\right]q_{\alpha} \end{cases} \tag{11}$$

here the $S_j$denotes the element j, and if the αth node in the element j coincides with the$i$th node, $\sigma(P_i,P_{\alpha}) = 1$; Else $\sigma(P_i,P_{\alpha}) = 0$. In the implementation, we only need to replace the corresponding terms in Eq. (11) by regularization terms.

3 The multipole expansion formulations

The formulations of the multipole expansion for half space acoustic problems are described in this section for 3D case.

3.1 The multipole expansion formulations for Helmholtz problems

The fundamental solution $G(x,x',y)$ for Helmholtz equation in 3-D can be expanded into the following series:

$$G(x,x',y) = \frac{ik}{4\pi}\sum_{n=0}^{\infty}(2n+1)\sum_{m=-n}^{n}\overline{I_n^m}(k,y-y_c)[O_n^m(k,x-y_c)+O_n^m(k,x'-y_c)],$$

$$|y-y_c| < |x-y_c|, \tag{12}$$

in which, y_c is an expansion point near y, and the function I_n^m and O_n^m can be expressed as:

$$\begin{cases} I_n^m = j_n(k|x|)Y_n^m(\frac{x}{|x|}) \\ O_n^m = h_n^{(1)}(k|x|)Y_n^m(\frac{x}{|x|}) \end{cases} \tag{13}$$

where $\overline{I_n^m}$ is the complex conjugate of I_n^m. $h_n^{(1)}$ and j_n are the nth order spherical Hankel function of first kind and nth order spherical Bessel function, respectively. Y_n^m denotes the spherical harmonics function which can be written as:

$$Y_n^m(x) = \sqrt{\frac{(n+m)!}{(n-m)!}}P_n^m(\cos\theta)e^{im\psi}, \tag{14}$$

here the coordinates of x in a spherical coordinate system is $(.\rho,.\theta,.\psi)$. P_n^m is the associated Legendre function.

With applying the expansion (13), we can evaluate the integral with kernel $G(x,x',y)$ in Eq.(1) through the following equation:

$$\int_{S_c} G(x,x',y)q(y)dS(y) = \frac{ik}{4\pi}\sum_{n=0}^{\infty}(2n+1)\sum_{m=-n}^{n}M_{n,m}(k,y_c)[O_n^m(k,x-y_c)+O_n^m(k,x'-y_c)],$$

$$|y-y_c| < |x-y_c|, \tag{15}$$

$$\int_{S_c}\frac{\partial G(x,x',y)}{\partial n}q(y)dS(y) = \frac{ik}{4\pi}\sum_{n=0}^{\infty}(2n+1)\sum_{m=-n}^{n}H_{n,m}(k,y_c)[O_n^m(k,x-y_c)+O_n^m(k,x'-y_c)],$$

$$|y-y_c| < |x-y_c|, \tag{16}$$

where $M_{n,m}(k,y_c)$ and $H_{n,m}(k,y_c)$ denote the multipole moments centered at y_c, their forms are:

$$M_{n,m}(k,y_c)=\int_{S_c}\overline{I_n^m}(k,y-y_c)q(y)dS(y), \tag{17}$$

$$H_{n,m}(k,y_c)=\int_{S_c}\frac{\partial\overline{I_n^m}(k,y-y_c)}{\partial n}\phi(y)dS(y), \tag{18}$$

3.2 Multipole conversion

When the multipole moments center shifts y_c to $y_{c'}$, which is called moment to moment (M2M) translation, the multipole moments are translated according to the following form:

$$M_{n,m}(k,y_{c'})=\sum_{n'=0}^{\infty}(2n'+1)\sum_{m'=-n'}^{n'}\sum_{\substack{l=|n-n'|\\ n'+n-l:even}}^{n+n'}(-1)^{m'}W_{n,n',m,m',l}I_l^{-m-m'}(k,y_c-y_{c'})M_{n',-m'}(k,y_c), \tag{19}$$

where $W_{n,n',m,m',l}$ is calculated by the following formula:

$$W_{n,n',m,m',l}=(2l+1)i^{n'-n+l}\begin{pmatrix} n & n' & l \\ 0 & 0 & 0\end{pmatrix}\begin{pmatrix} n & n' & l \\ m & m' & -m-m'\end{pmatrix}, \tag{20}$$

and $\begin{pmatrix} \bullet & \bullet & \bullet \\ \bullet & \bullet & \bullet\end{pmatrix}$ denotes the Wigner 3j symbol.

The local expansion for the $G(x,x',y)$integral in Eq. (1) can be described as the following form:

$$\int_{S_c}G(x,x',y)q(y)dS(y)=\frac{ik}{4\pi}\sum_{n=0}^{\infty}(2n+1)\sum_{m=-n}^{n}L_{n,m}(k,y,x_L)\overline{I_n^m}(k,x-x_L), \tag{21}$$

In the moment to local (M2L) translations, the local expansion coefficients are given by the following form:

$$L_{n,m}(k,y,x_L)=\sum_{n'=0}^{\infty}(2n'+1)\sum_{m'=-n'}^{n'}\sum_{\substack{l=|n-n'|\\ n'+n-l:even}}^{n+n'}W_{n',n,m',m,l}N_l^{-m-m'}(k,x_L-y_c)M_{n',m'}(k,y_c),$$
$$|x-x_L|<|y_c-x_L|, \tag{22}$$

here x_L is the local expansion center and N_n^m is defined as:

$$N_n^m=h_n^{(1)}(k|x|)\overline{Y_n^m}(\frac{x}{|x|}), \tag{23}$$

If the local expansion center shifts form x_L to $x_{L'}$, the form of the L2L translation is:

$$L_{n,m}(k,y,x_L) = \sum_{n'=0}^{\infty}(2n'+1)\sum_{m'=-n'}^{n'}\sum_{\substack{l=|n-n'|\\ n'+n-l:even}}^{n+n'} W_{n',n,m',-m,l} I_l^{m-m'}(k,x_{L'}-x_L) L_{n',m'}(k,y,x_L), \tag{24}$$

M2M, M2L, L2L translations are illustrated in Fig. 2.

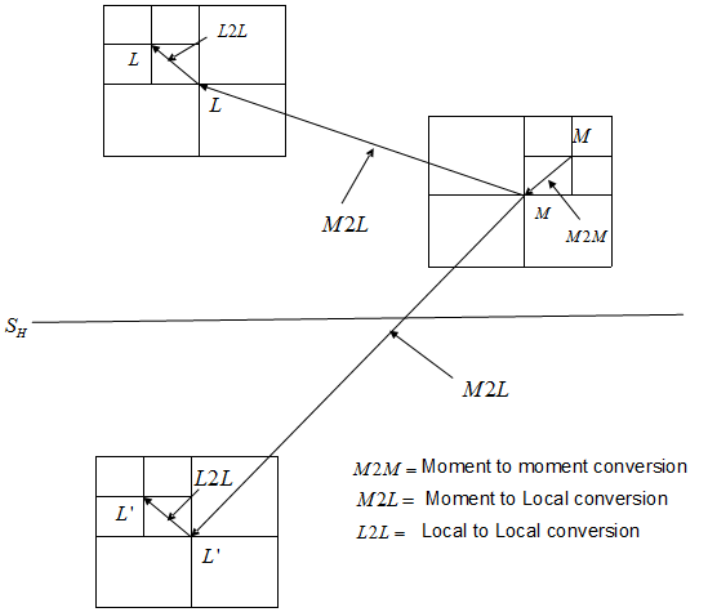

Figure 2: Conversion of the FMM: M2M, M2L, L2L translations

Similar translation can be applied in calculation of the integrals in Eq. (7).

Finally, we substitute the above FMM formulations to Eq. (8), for the ith node x, and the αth node which is in the jth element, the related term in Eq. (8) can be evaluated using the local expansion:

$$h_{ij}^{\alpha}\phi_{\alpha} \quad or \quad g_{ij}^{\alpha}q_{\alpha} \quad = \frac{ik}{4\pi}\sum_{n=0}^{\infty}(2n+1)\sum_{m=-n}^{n} L_n^m(k,y_{\alpha},x_L)[\overline{I_n^m}(k,x_L) + \beta\frac{\partial\overline{I_n^m}(k,x_L)}{\partial n_0}], \tag{25}$$

here x is far away from any point in element j. To calculate the integral over the elements which are near the field point x, the conventional Gaussian numerical integration method is applied in this paper.

Since only the real boundary discretization is required, the adaptive tree structure is constructed in the real domain in the half space adaptive FMBFM. And the adaptive tree structure is the same as that in the full space adaptive FMBFM (Wang et al., 2013). The block diagonal pre-conditioner used in the GMRES is calculated once, and then stored for all iterations. This work can further improve the efficiency of the FMBFM.

4 Numerical results

The proposed techniques have been implemented in C++. In this section, three numerical examples are presented to demonstrate the performance of the method. For the purpose of error estimation, a formula is defined as

$$e = \frac{1}{|u|_{\max}} \sqrt{\frac{1}{N} \sum_{i=1}^{N} (u_i^{(e)} - u_i^{(n)})^2} \tag{26}$$

where $u_i^{(e)}$ and $u_i^{(n)}$ refer to the exact and numerical solutions respectively and $|u|_{\max}$ is the maximum value of $u$over N nodes.

All the computations are performed on a PC with an Intel(R) Dual-Core CPU (2.6 GHZ) and 2GB memory. The rigid half space plane is the plane z=0 in all the examples in this paper. In all the numerical examples, the sound pressure ϕ we used is complex value. The maximum number of the quadratic elements in leafs is 20. The multipole expansion terms p is 6. In the GMRES solver, we stop the iteration when the relative error is less than 10^{-4}.

4.1 Validation of the half space adaptive FMBFM

As the first numerical example, a half sphere (Fig. 3) is analyzed to demonstrate the validity of the half space adaptive FMBFM for acoustic problems in an half infinite acoustic domain. The radius of the half sphere is a=1, and centered at (0, 0, 0). The wave number is k=π. The half sphere is modeled by 160 sphere surface elements and 246 contact surface elements. The half sphere is impinged upon by a plane incident wave traveling in the +x direction. This example is equivalent to the example a sphere impinged upon by a plane incident wave traveling in the +x direction in the full space. The analytical solution to this problem can be expressed by:

$$\phi^s(r,\theta) = \sum_{m=0}^{\infty} -\frac{i^m(2m+1)j'_m(ka)}{h'_m(ka)} P_m(\cos\theta) h_m(kr), \tag{27}$$

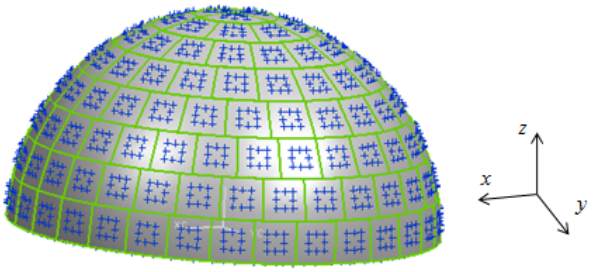

Figure 3: A half sphere model, which is meshed with 160 sphere surface elements

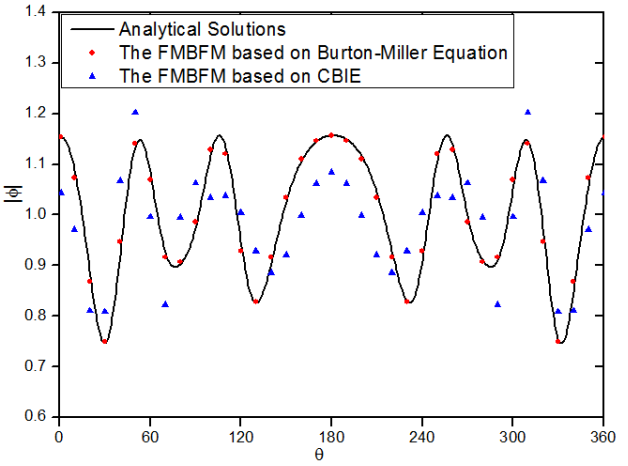

Figure 4: Pressure at r=3a from the scattering sphere at the wave number$k$=π.

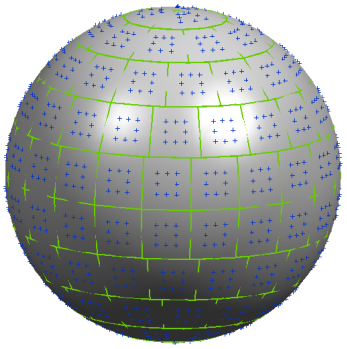

Figure 5: A rigid ball modeled with 136 elements

where$r$ is the distance between the computed point and the center of the sphere, θ is an angle from the direction of the incoming wave. P_m is the Legendre function of the first kind. h_m denotes the spherical Hankel function of the first kind. Fig. 4 shows the variation of sound potential ϕ at a distance r=3a, which is plotted versus the polar angle θ. The wave number in this problem is a characteristic wave number, which satisfies ka=π and under which the CBIE usually suffers from the non-uniqueness solution problem (The results obtained by the half space adaptive FMBFM based on CBIE (blue dots) are shown in Fig. 4). From the Fig. 4, we identify again that the results obtained by the half space adaptive FMBFM based on the Burton-Miller equation coincide with the analytical solutions. It demonstrates that the non-uniqueness difficulty of acoustic problems at the characteristic frequency can be circumvented by the half space adaptive FMBFM with CHBIE. Moreover, the results demonstrate that the half space adaptive FMBFM with quadratic elements is accurate.

Furthermore, a unit rigid ball model (Fig. 5) is plotted to verify the adaptive FMBFM for radiation problems. The rigid ball is meshed with 136 discontinuous quadrilateral quadratic elements (1088 nodes). The results of half space adaptive FMBFM are compared with those of full space. The wave number k=0.5, The boundary condition on the sphere is the Neumann boundary condition with the value given by (0.0, -207.515). The results from full space here is come from the results in Reference (Wu et al., 2012), denoted by $||\phi||$M. The results of half space FMBFM is $||\phi||$. The distance h between the center of the sphere and the rigid plane varies from 0 to 10. The case when h=0 indicates that the sphere is cut into two parts by the z=0 plane, as in the Fig. 3. The analytical result is available for the first case when h=0, that is, $||\phi||$=37.1214. Table 1 shows the results for the radiating sphere model. It shows that the results of half space adaptive FMBFM is in agreement with those of full space. Especially in the case h=0, the results of half space adaptive FMBFM agree with the analytical very well. In addition, the number of elements used in half space adaptive FMBFM is only half of the that in full space for noncontact case. This example indicates that the half space adaptive FMBFM with quadratic elements is an efficient tool for both contact and noncontact half space acoustic problems.

Table 1: Results for the radiating sphere model

Distance h	h=0	h=2	h=5	h=10
$\|\|\phi\|\|$	37.1204	70.291	52.1029	33.4164
$\|\|\phi\|\|_M$	37.1061	70.2517	52.0589	33.3992

4.2 Performance study of the half space adaptive FMBFM

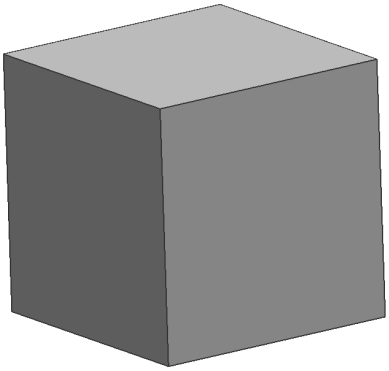

Figure 6: A simple block model

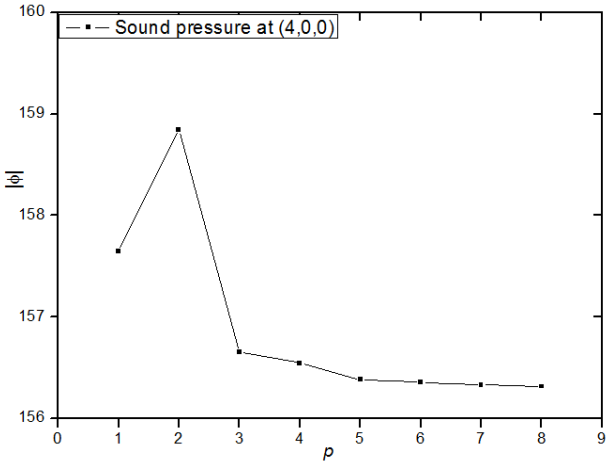

Figure 7: The influence of the multipole expansion terms for the sound pressure at (4,0,0)

In order to further study the performances of the half space adaptive FMBFM with quadratic elements, a pulsating block model (Fig. 6), which occupies in [-0.5,0.5]×[-0.5,0.5]×[0,1.0], with wave number k=5.0, is used for illustrating the accuracy of the half space adaptive FMBFM. The block contacts with the plane z=0. The boundary condition for the model is normal velocity v_0=1.0, ρ=1.22 kg/m3 and the sound velocity c=340.0 m/s. The overall dimensions of the model

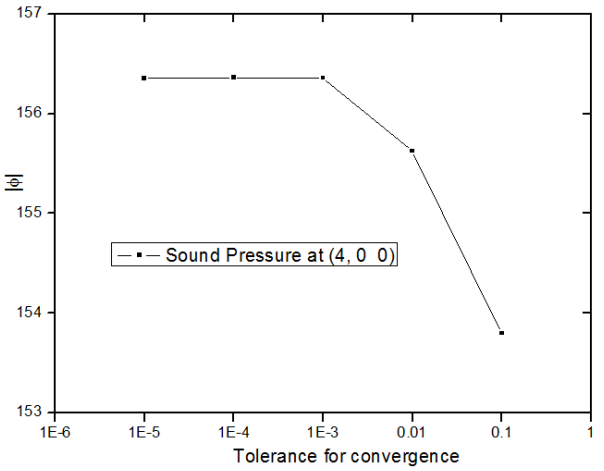

Figure 8: The influence of the tolerance for the sound pressure at (4,0,0)

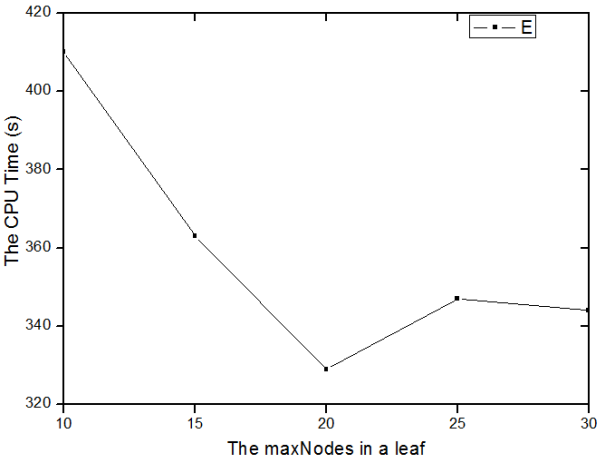

Figure 9: The influence of the max number of nodes in a leaf for the CPU time

are [-0.5,0.5]×[-0.5,0.5]×[0,1.0] in x, y, z directions, respectively. Fig. 7 shows the influence of the number of multipole expansion terms for the sound pressure. From the Fig. 7 we identify clearly that the numerical value of sound pressure become stabilization at p=5. Fig. 8 shows the influence of the tolerance for the sound pressure. From the Fig. 8 we identify clearly that the numerical value of sound pressure become stabilization at 10^{-3}. Fig. 9 shows the influence of the max number of nodes in a leaf for the CPU time. From the Fig. 9 we identify clearly that

less CPU time is consumed when the max number of nodes in a leaf is 20. Thus in this paper we set the multipole expansion terms p=6, the tolerance for convergence is 10^{-4}, and the max number of elements in a leaf is 20.

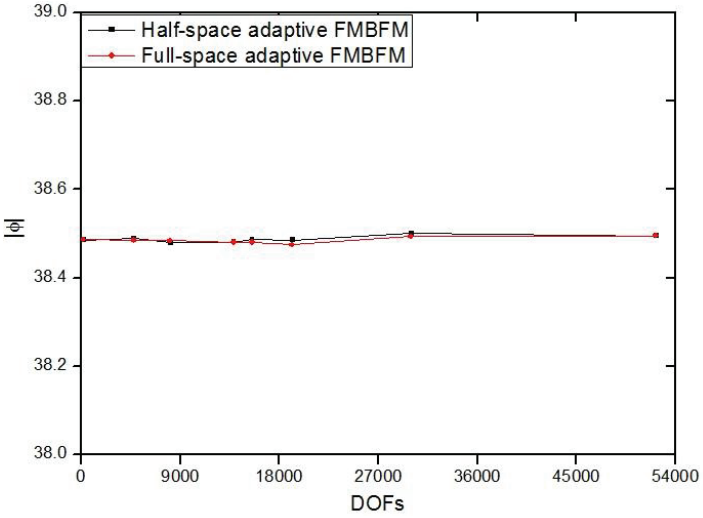

Figure 10: The pressure from the half space and form the full space FMBFM.

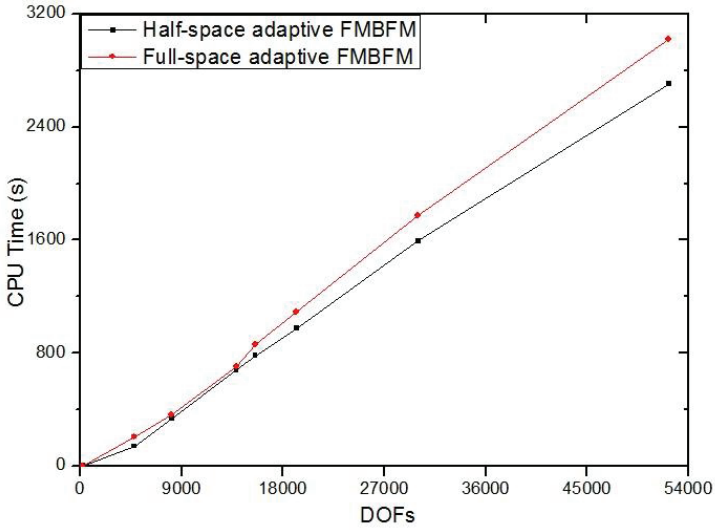

Figure 11: The CPU time used for the half-space and for full-space FMBFM.

Then, we test the performances of the half space adaptive FMBFM and the full space adaptive FMBFM. Here, the DOFs denotes the number of nodes in the model shown in Fig .6, and the mesh size in the corresponding full space model is the same as that in the half space. The wave number k=0.5. The sound potentials for the sample point (4, 0, 0) are shown in Fig. 10. From the Fig. 10, we identified clearly that the results obtained by the half space FMBFM coincide with the results obtained by full space FMBFM. The CPU time consumed in two methods is compared in Fig. 11. As shown in Fig. 11, the half-space FMBFM consumes less total CPU time than the full space FMBEM, especially for a large number of nodes. Fig.11 also indicates suggests the O(NlogN) efficiency of the presented method. This example demonstrates that the half space FMBFM is accurate and more efficient than the full space FMBFM.

4.3 Sound barrier models

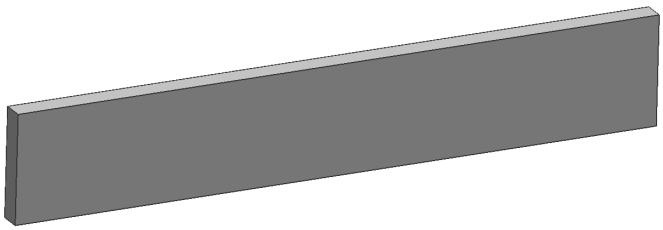

Figure 12: Half space sound barriers model

In the final example, the influence of a sound barrier (Fig. 12) placed between a point source and the sound field is tested using the half space adaptive FMBFM. The sound barrier is [5, 6]×[-15, 15]×[0, 5] in x, y, z directions, respectively. The 2D diagram of the sound barriers and sound field is show in Fig. 13. The incident point source is placed at (0, 0, 1) in 3D space. The wave number is k=1. In total 2478 quadrilateral quadratic elements (19824 nodes) are employed to mesh the model. The number of the field points in this example is 516. And all the field points locate on the quadrangle area which are [16, 26]×[-5, 5] in z=0 plane. Fig. 14 shows the contour plot of the dB on the back surface of the barrier with respect to the source. Fig. 15 gives the sound pressure level in decibel when no barrier is present. Fig. 16 shows the contour plot of the dB on the sound field with barrier. It consumes 2480s for computation of the sound field with barrier. From the contour we can identify that the sound pressure decreases a lot owing to the barrier. The maximum of the sound pressure is 77.32dB without barrier, but only 67.96dB with the barrier. The results and performance of the adaptive half space FMBFM

in simulations of the sound barrier shows that the half space adaptive FMBFM is efficient and able to handle practical problems.

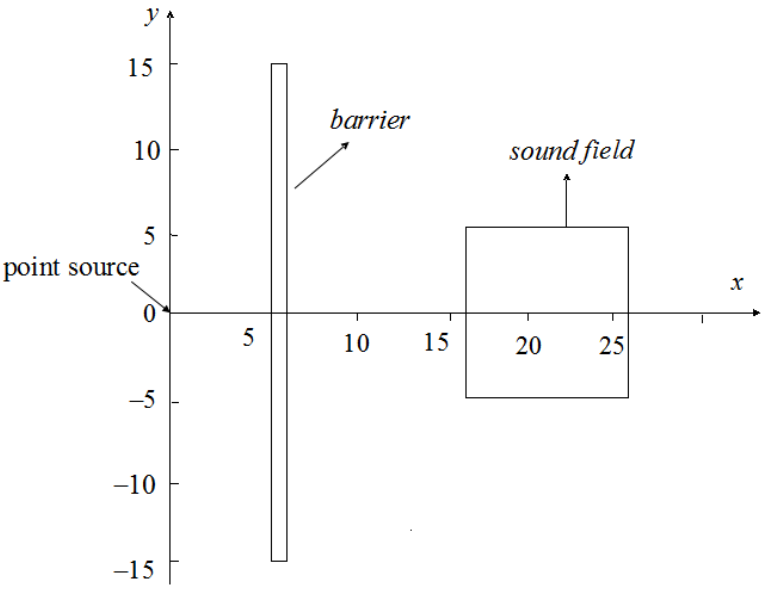

Figure 13: Half space sound barriers model and sound field (2D view)

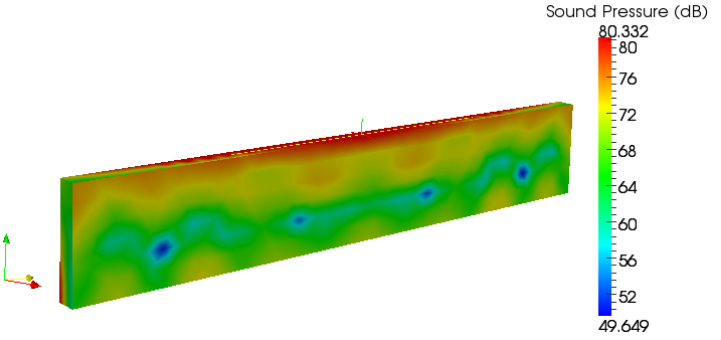

Figure 14: Contour plot of sound pressure level (dB) on the sound barrier.

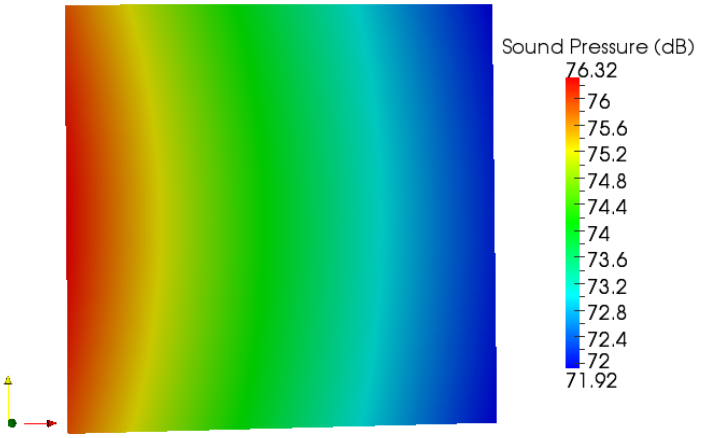

Figure 15: Contour plot of sound pressure level (dB) on the sound field without barrier.

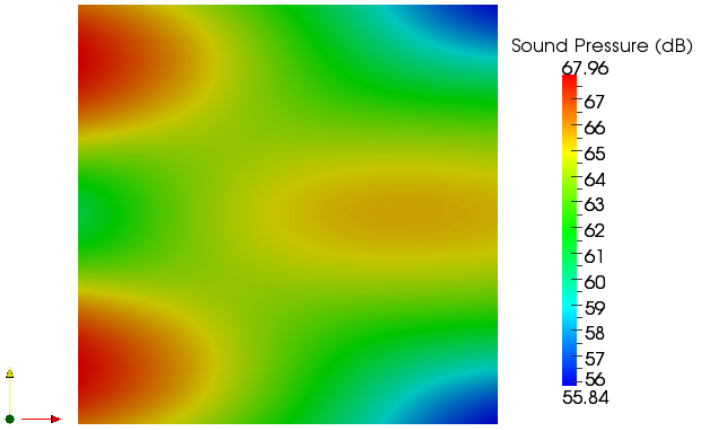

Figure 16: Contour plot of sound pressure level (dB) on the sound field with barrier.

5 Conclusions and discussion

In this paper, a half space adaptive fast multipole boundary face method with higher order elements is presented to solve the half space exterior acoustic problems in 3D. The half-space Green's function is adopted in the BIE formulation, thus the discretisation of the boundary is only necessary for the boundaries of the real domain, which ensures that the tree structure in the FMBFM can be constructed in the real domain only. The Burton-Miller equation is used in this paper to circumvent the problem of non-unique solution. The results of the numerical examples demonstrate the efficiency and validity of the half space adaptive FMBFM for acoustic radiation and scattering problems. The memory usage and CPU time in the half space adaptive FMBFM are less than that in the full-space FMBFM.

The most exciting feature of our method, perhaps, is that it unifies the CAD model and CAE into a unique framework and thus has potential to offer very promising applications in practical engineering. However, the FMM used in this paper is the original FMM (Epton et al, 1995), incorporating with the new FMM (Rokhlin, 1993) is ongoing. Moreover, a solution for problems on multi-domains is also ongoing.

Acknowledgments

This work was supported by National Science Foundation of China under grant numbers 11172098, and in part by Hunan Provincial Natural Science Foundation for Creative Research Groups of China (Grant No.12JJ7001).

References

Aoki, S.; Amaya, K.; Urago, M.; Nakayama, A. (2004): Fast multipole boundary element analysis of corrosion problems. *CMES-Comput. Model. Eng. Sci.,* vol. 6, no. 2, pp. 123-132.

Bapat, M.S.; Shen, L.; Liu, Y.J. (2009): Adaptive fast multipole boundary element method for three-dimensional half-space acoustic wave problems. *Eng. Anal. Bound. Elem.,* vol. 33, pp. 1113–1123.

Bapat, M.S.; Liu, Y.J. (2010): A new adaptive algorithm for the fast multipole boundary element method. *CMES-Comput. Model. Eng. Sci.,* vol. 58, No. 2, pp. 161-184.

Brancati, A.; Aliabadi, M. H.; Benedetti, I. (2009): Hierarchical adaptive cross approximation GMRES technique for solution of acoustic problems using the boundary element method. *CMES-Comput. Model. Eng. Sci.,* vol. 43, no. 2, pp. 149-172.

Brunner, D.; Junge, M.; Rapp, P.; Bebendorf, M.; Gaul, L. (2010): Comparison of the fast multipole method with hierarchical matrices for the Helmholtz-BEM. *CMES-Comput. Model. Eng. Sci.*, vol. 58, pp. 131–160.

Burton, A.J.; Miller, G.F. (1971): The application of integral equation methods to numerical solution of some exterior boundary value problem. *Proc. R. Soc. London A*, vol. 323, pp. 201-210.

Cao, Z.Y.; Zhu, J.X.; Cheung, Y.K. (1990): A semi-analytical boundary element method for scattering of waves in a half space. *Earthquake Engng. Struct. Dyn.*, vol.19, pp.1073-1082.

Chen, X.L.; Liu, Y.J. (2001): Thermal stress analysis of multi-layer thin films and coatings by an advanced boundary element method. *CMES-Comput. Model. Eng. Sci.,* vol. 2, no. 3, pp. 337-350.

Epton, M.A.; Dembart, B. (1995): Multipole translation theory for the three-dimensional Laplace and Helmholtz equations. *SIAM J. Sci. Comput.,* vol. 16, pp. 865-97.

Frangi, A.; Bonnet, M. (2010): On the fast multipole method for the Helmholtz equation with complex frequency. *CMES-Comput. Model. Eng. Sci.,* vol. 58, pp. 271-291.

Greengrad, L.; Rokhlin, V. (1987): A fast algorithm for particles simulations. *J. Comput. Phy.,* vol. 73, pp. 325-348.

Gu, J.L.; Zhang, J.M.; Sheng, X.M.; Li, G.Y. (2011): B-spline approximation in boundary face method for three-dimensional linear elasticity. *Eng. Anal. Bound. Elem.,* vol. 35, pp. 1159-1167.

Liu, Y.J.; Chen, S.H. (1999): A new form of the hyper-singular boundary integral equation for 3-Dacoustics and its implementation with C0 boundary element. *Comput. Methods Appl. Mech. Eng.,* vol. 173, pp. 375-386.

Meyer, W.L.; Bell, W.A.; Zinn, B.T.; Stallybrass, M.P. (1978): Boundary integral solutions of three dimensional acoustic radiation problems. *J. Sound Vib.,* vol. 59, pp. 245-262.

Mukherjee, Y.X.; Mukherjee, S. (1997): The boundary node method for potential problems. *Int. J. Numer. Meth. Eng.*, vol. 40, pp. 797-815.

Qian, Z.Y.; Han, Z.D.; Atluri, S.N. (2013): A Fast Regularized Boundary Integral Method for Practical Acoustic Problems. *CMES-Comput. Model. Eng. Sci.*, vol. 91, no. 6, pp. 463-484.

Qin, X.Y.; Zhang, J.M.; Li, G.Y.; Sheng, X.M.; Song, Q.; Mu, D.H. (2010): An element implementation of the boundary face method for potential problems in three dimensions. *Eng. Anal. Bound. Elem.,* vol. 34, pp. 934-943.

Rokhlin, V. (1985): Rapid solution of integral equations of classical potential theory. *J. Comput. phy.*, vol. 60, pp. 187-207.

Rokhlin, V. (1993): Diagonal forms of translation operators for the Helmholtz equation in three dimensions. *Appl. and Comput. Harmon. Anal.*, vol. 1, pp. 82-93.

Seçgin, A.; Sarıgül, A.S. (2010): An efficient sound source determination process based on half-space boundary element method. *Int. J. Mech. Mater. Des.,* vol. 6, pp. 17-25.

Seybert, A.F.; Soenarko, B. (1988): Radiation and scattering of acoustic waves from bodies of arbitrary shape in three-dimensional half space. *ASME Trans J. vib. Acoust. Stress Reliab. DES.,* vol. 110, pp. 112-17.

Shen, L.; Liu, Y.J. (2007): An adaptive fast multipole boundary method for three-dimensional acoustic wave problems based on the Burton-Miller formulation. *Comput. Mech.,* vol. 40, pp. 461-72.

Wang, H.T.; Yao, Z.H. (2005): A new fast multipole boundary element method for large scale analysis of mechanical properties in 3D particle-reinforced composites. *CMES-Comput. Model. Eng. Sci.,* vol. 7, no.1, pp. 85-96.

Wang, Q.; Miao, Y.; Zhu, H. P.; Zhang, C. (2012): An O(N) fast multipole hybrid boundary node method for 3D elasticity. *Comput. Mater. Continua*, vol. 28, no. 1, pp. 1-26.

Wang, X.H.; Zhang, J.M.; Zhou, F.L.; Zheng, X.S. (2013): An adaptive fast multipole boundary face method with higher order elements for acoustic problems in three-dimension. *Eng. Anal. Bound.Elem.,* vol. 37, pp. 144-152.

Wu, H.J.; Liu, Y.J.; Jiang, W.K. (2012): Analytical integration of the moments in the diagonal form fastmultipole boundary element method for 3-D acoustic wave problems. *Eng. Anal. Bound.Elem.,* vol. 36, pp. 248-54.

Zhang, J.M., Qin, X.Y., Han, X.; Li, G.Y. (2009): A boundary face method for potential problems inthree dimensions. *Int. J. Numer. Meth. Eng.,* vol. 80, pp. 320-337.

Zhang, J.M.; Yao, Z.H. (2001): Meshless Regular Hybrid Boundary Node Method. *CMES-Comput. Model. Eng. Sci.*, vol.1, no.1, pp.1-12.

Zhang, J.M.; Tanaka Masa. (2006): An effective tree data structure in fast multipole method. *Transactions of JASCOME.,* vol. 6, pp. 17-22.

Zhang, J.M.; Tanaka Masa. (2007): Adaptive spatial decomposition in fast multipole method. *J.Comput. Phy.,* vol. 22, pp. 617-28.

Zhou, F.L.; Zhang, J.M.; Sheng, X.M.; Li, G.Y. (2011): Shape variable radial basis function and itsapplication in dual reciprocity boundary face method. *Eng. Anal. Bound. Elem.*, vol. 35, pp. 244-252.